Topological equivalence of stomata distribution patterns across vascular plants

Paulette I Naulin[a] & Sergio A Estay[b,c] *

[a] Universidad de Chile, Laboratorio Biología de Plantas, Departamento de Silvicultura y Conservación de la Naturaleza, Av. Santa Rosa 11315, La Pintana, Santiago, Chile.

[b] Instituto de Ciencias Ambientales y Evolutivas, Facultad de Ciencias. Universidad Austral de Chile, Casilla 567, Valdivia, Chile.

[c] Center for Applied Ecology and Sustainability, Facultad de Ciencias Biológicas. Pontificia Universidad Católica de Chile. Santiago 6513677, Chile

* **Corresponding author**: sergio.estay@uach.cl

Summary

Stomata are ancient anatomical structures on leaves that regulate the exchange of water vapor, oxygen, and carbon dioxide between plants and the atmosphere. Acting as valve-like gateways between internal tissues and the external environment, stomata may function as locally interacting networks. Theoretical and experimental evidence suggests that local interactions among neighboring stomata influence their function and spatial arrangement. From this perspective, analyzing stomatal distributions as networks may yield novel insights into observed spatial patterns and their generative mechanisms. We hypothesize that variability in stomatal arrangements arises from shared underlying rules, with observed diversity reflecting an epiphenomenon. To test this, we employed a multi-species, multi-site common garden approach to assess potential convergences in stomatal distribution. A network-based framework enabled us to reduce individual-level variability and analyze stomatal patterns as interacting systems. Our results show that, across species and environments, stomatal spatial configurations consistently align with a null model linking minimum spanning tree (MST) length to stomatal density. Although a variety of patterns were present, over-dispersed arrangements predominated. These findings suggest that physical constraints during stomatal development impose strong limits on the range of viable spatial configurations that can evolve.

Keywords: stomata patterning, minimum spanning tree, scaling, leaf architecture, spatial networks

Introduction

Stomata are ancient anatomical structures on leaves that regulate the exchange of gases—water vapor, oxygen, and carbon dioxide—between plants and the atmosphere (Edwards et al., 1998; Croxdale, 2001; Hetherington & Woodward, 2003; Bergmann, 2004; Matkowski & Daszkowska-Golec, 2023). Traits such as stomatal size, density, shape, and spatial distribution vary widely among individuals, species, and environments. For example, stomatal size (often measured as pore length) has been found to correlate weakly with latitude, although the specific environmental drivers behind this pattern remain unclear (McKown et al., 2014). Results from common garden experiments suggest that pore size may co-vary with climatic conditions (Carlson et al., 2016). These findings support the idea that stomatal traits exhibit a degree of plasticity, with potentially important implications for plant physiological performance (Drake et al., 2013).

Stomatal density is the simplest and most commonly used descriptor of their spatial distribution on the leaf surface. For instance, McKown et al. (2014) reported that stomatal density in Populus species is negatively correlated with both temperature and precipitation across a latitudinal gradient. In contrast, Fontana et al. (2017) observed a slightly positive relationship between stomatal density and rainfall in *Salix miyabeana*, highlighting the complexity of environmental influences. Beyond temperature and precipitation, other factors also appear to modulate stomatal density. Antunes de Almeida Filho et al. (2017) found that the distance between neighboring stomata, likely influenced by overall density, increased with light exposure, suggesting that light availability can also shape stomatal spatial patterns.

Stomatal spatial arrangement has traditionally been described as uniform, with distinct "stomata-free" regions surrounding each stoma (Sachs, 1991). However, Naulin et al. (2017) demonstrated that this perception may be an artifact of the point-pattern analysis methods commonly employed in such studies. By applying a more realistic disc-pattern analysis, they showed that stomatal distributions can span the full theoretical spectrum—from uniform to random to clustered patterns. To fully understand stomatal organization and its underlying mechanisms, spatial patterning must be explicitly analyzed. Various biological (e.g., genetic) and physico-chemical mechanisms, such as activation–inhibition processes, appear to regulate stomatal spacing to avoid configurations that impair stomatal function (Serna & Fenoll, 1997; Illian et al., 2008; Dow et al., 2013; Fanourakis et al., 2015; Fiorin et al., 2015).

Thus, stomatal distribution can be considered an anatomical trait subject to strong ecological and evolutionary pressures (e.g., Fiorin et al., 2015; Xiong & Flexas, 2020).

Variability in stomatal spatial arrangements may—or may not—have an evolutionary basis. Evidence from common garden experiments indicates that intraspecific variation in stomatal density can be adaptive. For example, Carlson et al. (2016) identified a positive selection gradient favoring individuals with stomatal traits suited to drier and hotter environments. At the interspecific level, Yang et al. (2023) analyzed 90 species and found that, depending on the spatial scale, both aggregated and uniform (i.e., over-dispersed) stomatal distributions exhibit weak phylogenetic signals, suggesting a partial influence of evolutionary history. While these studies offer valuable insights, the relative contributions of evolutionary and environmental factors in shaping stomatal density and distribution remain unclear. Zhang et al. (2012), for instance, reported species-specific responses: in some species, stomatal traits were predominantly shaped by environmental conditions, whereas in others, genetic control was more pronounced.

The spatial and temporal context in which a leaf develops plays a crucial role in shaping stomatal density and distribution. Even today, variation in these traits is used to infer past environmental conditions, particularly in palaeobotanical records (e.g., Uhl & Kerp, 2005). Conceptually, stomata function as windows that connect internal leaf tissues with the external environment. Each stoma can be thought of as a valve-like structure that regulates gas exchange within a specific region of the leaf surface (Clark et al., 2022). Both theoretical and experimental studies have shown that stomatal function is influenced by neighboring stomata (Haefner et al., 1997; Mott et al., 1997). These local interactions suggest that stomatal arrangements operate as locally interacting networks. If this is the case, analyzing stomatal distributions and their structural properties through a network-based framework could offer novel insights into the spatial patterns observed and the underlying generative mechanisms. We therefore hypothesize that the apparent variability in stomatal distributions arises from shared generative rules, and that the diversity of observed patterns may simply be an epiphenomenon.

In this study, we apply a multi-species, multi-site common garden approach to identify potential commonalities in observed stomatal distribution patterns. By using a network-based

framework, we minimize the confounding effects of individual variability and treat stomatal arrangements as interacting biological systems.

Methods

Biological data

Sixty-six plant species, spanning four classes, 27 orders, and 41 families, were sampled from two arboreta: the Antumapu Arboretum (hereafter Antumapu; 33.57°S, 70.63°W) and the Frutillar Arboretum (hereafter Frutillar; 41.12°S, 73.03°W), both managed by the Faculty of Forestry and Nature Conservation, University of Chile (Table S1). These sites are approximately 980 km apart. Antumapu is located in a warm-summer Mediterranean climate (Köppen classification: Csb), with average summer and winter temperatures of 19°C and 9.5°C, respectively, and an annual precipitation of 371 mm (Santibañez, 2017). In contrast, Frutillar is situated in southern Chile within a temperate oceanic climate (Köppen classification: Cfb), characterized by average summer and winter temperatures of 14.3°C and 7°C, respectively, and an annual precipitation of 1516 mm (Santibañez, 2017).

For each species, three fully developed leaves were collected. Leaves were cleared following the protocol described by Castellaro et al. (2007) and mounted on glass slides for microscopic examination and imaging. After processing, a total of 180 samples were available for analysis. Anatomical measurements were performed using images of approximately 1 mm² from the central third of the abaxial leaf surface. To estimate spatial properties, the centroid of each stomatal complex was determined using Cartesian coordinates in ImageJ software (Rasband, 1997; Schneider et al., 2012). Additionally, the maximum and minimum diameters of 30 stomata were measured per sample, and the total number of stomata was recorded (Table S1).

Network reconstruction

As noted earlier, local interactions between stomata suggest that their spatial arrangements function as locally interacting networks. Our goal, therefore, is to define a method for constructing a graph that best represents these interactions among stomata. Based on the idea that each stoma connects a specific region of the leaf surface to the atmosphere, we estimated

this area using Voronoi polygons (Aurenhammer et al., 2013). In a Voronoi diagram, each polygon is centered on a stoma, and all points within that polygon are closer to the central stoma than to any other in the sampled area.

To represent potential local interactions, we connected neighboring polygons by linking the centroids of adjacent stomata. This process generates a Delaunay triangulation—the dual graph of the Voronoi diagram—which connects each stoma to its nearest neighbors, forming a dense network in which each node (stoma) typically has a degree of approximately six (Aurenhammer et al., 2013).

Within the Delaunay triangulation lies a key subgraph known as the Minimum Spanning Tree (MST). The MST is a loop-free graph that connects all nodes while minimizing the total edge length (Prim, 1957). In the context of complex spatial patterns, the MST is often used to characterize dominant connectivity structures. The MST has a long history of applications in biology and ecology, and its topological properties are well-documented (Dussert et al., 1986, 1987; Cantwell & Forman, 1993; Jones et al., 1996; Wallet & Dussert, 1997; Bunn et al., 2000; Urban et al., 2001; Dry et al., 2012). More recently, Liu et al. (2021) applied MST-based methods to the analysis of stomatal arrangements, making it an ideal starting point for identifying common structural features of stomatal distribution across plant species—particularly in light of the trade-off between epidermal space use for photosynthesis and water conservation (Lawson & McElwain, 2016).

MSTs exhibit a range of topological properties that can be used to classify spatial arrangements of objects. Metrics such as total MST length, mean edge length, and the standard deviation of edge lengths are commonly used to characterize spatial configurations (Hoffman & Jain, 1983; Dussert et al., 1989). Under the assumption of complete spatial randomness (i.e., a Poisson process) in two dimensions, the expected MST length approaches the following limit:

$$L_{mts} = \beta\,(N*A)^{1/2} \qquad (1)$$

where N is the number of points (stomata), A is the area of observation, and β is a constant that depends on the spatial structure of the distribution. Empirical estimates place β between 0.63 and 0.64 under random conditions (Beardwood et al., 1959; Bertsimas & Van Ryzin,

1990; Avram & Bertsimas, 1992; Jaillet, 1993; Cortina-Borja & Robinson, 2000). Values of β lower than this range indicate clustering, while higher values suggest over-dispersion.

In this study, we calculated the MST for each sample as a representation of the stomatal network. For each MST, we measured the total length and evaluated deviations from the null model (Equation 1) to infer differences in spatial arrangement.

To contextualize each sample, we compared its MST length to three simulated benchmark patterns: clustered, random (Poisson), and over-dispersed. Simulated patterns used the same number of stomata and observation area as the empirical sample. Clustered patterns were generated using four spatial clusters, while over-dispersed patterns applied a minimum inhibition distance equal to the mean stomatal diameter of the sample. Each scenario was simulated 1,000 times.

All analyses were conducted in R (2024), using the packages stpp (Gabriel et al., 2024), netgen (Bossek, 2025), and emstreeR (Quadros, 2025).

Results

Stomatal density across samples ranged from 3 to 777 stomata per mm². The lowest density was observed in a sample of the fern Asplenium trilobum, while the highest was recorded in Cryptocarya alba (Lauraceae). In general, higher stomatal densities were found in samples from the Mediterranean site (Antumapu), whereas stomatal diameter showed no consistent pattern between the two sites (Fig. 1; Table S2).

The same samples that exhibited the lowest and highest stomatal densities also showed the minimum and maximum MST lengths, with values ranging from 858 μm to 20,894 μm. As expected, there was a strong positive correlation between the number of stomata per sample and the total MST length (Pearson's r = 0.945; 95% CI: [0.927, 0.959]). Additionally, stomatal number was significantly negatively correlated with average stomatal diameter (r = –0.568; 95% CI: [–0.659, –0.459]).

Despite the three orders of magnitude variation in stomatal density, MST length across all samples was accurately predicted as a function of stomatal density, with a high coefficient of

determination ($R^2 = 0.94$; Fig. 1). However, the estimated value of the scaling parameter β was significantly higher than expected under complete spatial randomness. Specifically, we obtained a mean β of 0.7492 (95% CI: [0.7393, 0.7591]), which exceeds the typical range reported for Poisson-distributed patterns (0.63–0.64), suggesting a consistent tendency toward over-dispersion in stomatal spatial arrangements.

When comparing observed MST lengths against simulated distributions, 2.8% of the samples (5 out of 180) were classified as clustered, 27.2% (49 samples) as random, and 32.8% (59 samples) as over-dispersed. A total of 49.4% of the samples (89 samples) did not fall exclusively within any single category. This is due to overlapping confidence intervals, which allowed some samples to be classified into multiple categories.

Among the unclassified samples, 10% (18 samples) fell between the confidence intervals of the random and over-dispersed simulations, while 39.4% (71 samples) exceeded the upper limit of the over-dispersed range. In total, 72% of the samples (130 out of 180) either fell within or above the over-dispersed range, and 82% (148 samples) fell above the random distribution range.

No clear taxonomic pattern was observed in relation to the type of spatial arrangement. Full classification results for each sample are provided in Figures 2 and 3 and Table S2.

Discussion

Trade-offs and relationships among stomatal size, density, and spatial arrangement have garnered increasing attention over the past decade (e.g., Beerling & Franks, 2010; Brodribb et al., 2014). The diverse patterns reported in the literature appear to result from a still poorly understood interplay of genetic and environmental factors (Zhang et al., 2012). In this study, we collected data from a broad range of species growing in two ecologically contrasting environments. The stomatal density values observed in our samples were consistent with previous findings (Franks & Beerling, 2009; Haworth et al., 2023). Notably, the highest stomatal density and MST length were recorded in samples from the Mediterranean site (Antumapu) (Fig. 1), supporting the hypothesis that increased stomatal density under higher temperatures may represent an adaptive strategy to enhance gas exchange and evaporative cooling (Hill et al., 2015).

The strong positive correlation between stomatal density and MST length aligns with theoretical expectations from our model (Eq. 1): a greater number of nodes necessarily results in a longer minimum spanning tree (Beardwood et al., 1959; Cortina-Borja & Robinson, 2000). Furthermore, our findings are consistent with prior studies reporting a significant negative correlation between stomatal density and stomatal size across species (Franks & Beerling, 2009; Haworth et al., 2023).

However, when we focused on the subset of species present at both sites, we observed a more nuanced pattern (Table S2). With only one exception (*A. chilensis*), all species exhibited higher stomatal densities in the Mediterranean climate (Antumapu) compared to the temperate oceanic climate (Frutillar). In contrast, stomatal size did not follow a consistent trend across environments. These results suggest that, at the intraspecific level, stomatal density may be more responsive to environmental conditions than stomatal size—indicating a greater degree of plasticity. Nevertheless, this interpretation is based on a limited sample of seven species, and further studies with larger species pools are needed to confirm this pattern.

Although our dataset includes numerous species from diverse biogeographical origins and two ecologically distinct environments, the spatial configuration of stomata across all samples was well-described by the theoretical model (Eq. 1; Fig. 1). The strong fit of this model suggests that, across a wide range of lineages and taxonomic groups, stomatal arrangements adhere to a shared generative rule—one in which MST length scales with the square root of stomatal density and a constant parameter (β) representing spatial inhibition or repulsion among stomata. This result implies a form of topological equivalence across species and environments: the observed spatial patterns can be interpreted as scale transformations—shrinking or stretching—of a common underlying configuration.

At the spatial resolution of our analysis (~1 mm^2), no major deviations from this model were observed between species or sites. The estimated β value (>0.74) points to consistent repulsion or inhibition among stomata, aligning with both the "one-cell spacing" rule (Lawson & McElwain, 2016) and the finite-size constraint imposed by the physical dimensions of stomata themselves (Naulin et al., 2017). Our simulation results further support this interpretation. Although we examined a limited set of point process scenarios (single configurations for both clustered and over-dispersed patterns), the majority of

samples (72%) exhibited levels of over-dispersion equal to or greater than those generated by the over-dispersed simulations (Figs. 2–3).

As previously discussed, two main components likely contribute to this over-dispersion. First, stomata are not point-like objects—their finite size prevents overlap and inherently induces spatial repulsion (Naulin et al., 2017). Since our simulations are based on idealized point processes, part of the observed over-dispersion likely reflects this geometric constraint. Second, and more importantly, 39% of samples displayed levels of over-dispersion that exceeded our simulation range even after accounting for stomatal size. This suggests the presence of active biological mechanisms, likely of genetic origin, that enforce spatial inhibition during stomatal development—further supporting the view that stomatal patterns are shaped by endogenous regulatory processes in addition to biophysical constraints.

If our model accurately reflects the mechanisms governing stomatal spatial organization, it carries several important implications—both quantitative and qualitative—for understanding how stomata can be distributed on the epidermis. At low densities, there are potentially thousands of viable spatial configurations that achieve a functional balance in the trade-off between maximizing photosynthetic area and minimizing water loss. However, evolutionary increases in stomatal density not only force reductions in stomatal size (Franks & Beerling, 2009; Haworth et al., 2023), but also dramatically constrain the number of feasible spatial arrangements. Beyond a certain threshold, only over-dispersed configurations remain viable.

This constraint arises from fundamental geometric principles: the number of possible arrangements of finite-sized objects in a fixed area is far more limited than for point-like objects (Simberloff, 1979; Wu et al., 1987). As stomata cannot be infinitely small, increasing their number while preserving function requires increasingly regular spacing. In the theoretical limit, this constraint leads to a near-regular grid-like distribution.

It is important to note that these findings apply specifically to the spatial scale analyzed in this study (~1 mm^2). At broader spatial scales, additional structural constraints—such as those imposed by leaf venation networks—may further shape or override local stomatal arrangements (Matos et al., 2024). Future studies incorporating multiscale analyses and biomechanical modeling may provide deeper insights into how such hierarchical constraints interact across spatial levels.

Stomatal size and density are key determinants of CO_2 conductance in leaves (Franks & Beerling, 2009) and are therefore subject to strong selective pressures to balance mesophyll demand for carbon assimilation with efficient water vapor diffusion (Lawson & McElwain, 2016; Haworth et al., 2023). In a scenario of rising atmospheric CO_2 concentrations, species that already exhibit high stomatal densities may face increasingly limited options for allocating additional epidermal space to stomatal complexes due to geometric constraints. Our results suggest that further increases in stomatal density are only feasible through heightened over-dispersion, progressively driving stomatal arrangements toward grid-like spatial patterns across the leaf surface.

Acknowledgments

The authors acknowledge the financial support from ANID PIA/BASAL AFB240003

Author contributions

PIN and SAE conceived and planned the work. PIN performed sample preparation and digitalization. PIN and SAE analyzed the data. SAE wrote the manuscript and both authors commented on the draft.

Competing interests: Authors have no competing interests.

Data availability: all data is available as supporting information

References

Antunes de Almeida Filho H, Machicao J, Bruno OM. 2017. Geometric plasticity at leaves from *Ctenanthe oppenheimiana* probed by measure of distances between stomata. Journal of Physics: Conference Series 936: 012094.

Aurenhammer F, Klein R, Lee DT. 2013. Voronoi diagrams and Delaunay triangulations. Singapore: World Scientific Publishing Company.

Avram F, Bertsimas D. 1992. The minimum spanning tree constant in geometrical probability and under the independent model: a unified approach. Annals of Applied Probability 2: 113–130.

Beardwood J, Halton JH, Hammersley JM. 1959. The shortest path through many points. Mathematical Proceedings of the Cambridge Philosophical Society 55: 299–327.

Beerling DJ, Franks PJ. 2010. The hidden cost of transpiration. Nature 464: 495–496.

Bergmann DC. 2004. Integrating signals in stomatal development. Current Opinion in Plant Biology 7: 26–32.

Bertsimas DJ, Van Ryzin G. 1990. An asymptotic determination of the minimum spanning tree and minimum matching constants in geometrical probability. Operations Research Letters 9: 223–231.

Bossek J. 2024. netgen: Generating random (clustered) networks in R. R package version 1.3.2.

Brodribb TJ, McAdam SAM, Jordan GJ, Martins SCV. 2014. Conifer species adapt to low-rainfall climates by following one of two divergent pathways. Proceedings of the National Academy of Sciences, USA 111: 14489–14493.

Bunn AG, Urban DL, Keitt TH. 2000. Landscape connectivity: a conservation application of graph theory. Journal of Environmental Management 59: 265–278.

Cantwell MD, Forman RTT. 1993. Landscape graphs: ecological modeling with graph theory to detect configurations common to diverse landscapes. Landscape Ecology 8: 239–255.

Carlson JE, Adams CA, Holsinger KE. 2016. Intraspecific variation in stomatal traits, leaf traits and physiology reflects adaptation along aridity gradients in a South African shrub. Annals of Botany 117: 195–207.

Castellaro G, Squella F, Ullrich T, León F, Raggi A. 2007. Algunas técnicas microhistológicas utilizadas en la determinación de la composición botánica de dietas de herbívoros. Agricultura Técnica 67: 86–93.

Clark JW, Harris BJ, Hetherington AJ, Hurtado-Castaño N, Brench RA, Casson S et al. 2022. The origin and evolution of stomata. Current Biology 32: R539–R553.

Cortina-Borja M, Robinson T. 2000. Estimating the asymptotic constants of the total length of Euclidean minimal spanning trees with power-weighted edges. Statistics and Probability Letters 47: 125–128.

Croxdale J. 2001. Stomata. In: Encyclopedia of Life Sciences (ELS). Chichester, UK: John Wiley & Sons.

Dow GJ, Berry JA, Bergmann DC. 2014. The physiological importance of developmental mechanisms that enforce proper stomatal spacing in *Arabidopsis thaliana*. New Phytologist 201: 1205–1217.

Drake PL, Froend RH, Franks PJ. 2013. Smaller, faster stomata: scaling of stomatal size, rate of response, and stomatal conductance. Journal of Experimental Botany 64: 495–505.

Dry M, Preiss K, Wagemans J. 2012. Clustering, randomness and regularity: spatial distributions and human performance on the traveling salesperson problem and minimum spanning tree problem. The Journal of Problem Solving 4: 1–17.

435 Dussert C, Rasigni G, Rasigni M, Palmari J, Llebaria A. 1986. Minimal spanning tree: a new
436 approach for studying order and disorder. Physical Review B 34: 3528–3531.
437
438 Dussert C, Rasigni G, Rasigni M, Palmari J, Llebaria A, Marty F. 1987. Minimal spanning
439 tree analysis of biological structures. Journal of Theoretical Biology 125: 317–323.
440
441 Dussert C, Rasigni G, Rasigni M, Palmari J, Llebaria A. 1989. Minimal spanning tree
442 analysis of regular, random and cluster structures. Zeitschrift für Physik D 12: 41–44.
443
444 Edwards D, Kerp H, Hass H. 1998. Stomata in early land plants: an anatomical and
445 ecophysiological approach. Journal of Experimental Botany 49: 255–278.
446
447 Fanourakis D, Heuvelink E, Carvalho SM. 2015. Spatial heterogeneity in stomatal features
448 during leaf elongation: an analysis using *Rosa hybrida*. Functional Plant Biology 42:
449 737–745.
450
451 Fiorin L, Brodribb TJ, Anfodillo T. 2016. Transport efficiency through uniformity:
452 organization of veins and stomata in angiosperm leaves. New Phytologist 209: 216–227.
453
454 Fontana M, Labrecque M, Collin A, Bélanger N. 2017. Stomatal distribution patterns change
455 according to leaf development and leaf water status in *Salix miyabeana*. Plant Growth
456 Regulation 81: 63–70.
457
458 Franks PJ, Beerling DJ. 2009. Maximum leaf conductance driven by CO_2 effects on stomatal
459 size and density over geologic time. Proceedings of the National Academy of Sciences,
460 USA 106: 10343–10347.
461
462 Gabriel E, Rowlingson BS, Diggle PJ. 2013. stpp: an R package for plotting, simulating and
463 analyzing spatio-temporal point patterns. Journal of Statistical Software 53: 1–29.
464
465 Haefner JW, Buckley TN, Mott KA. 1997. A spatially explicit model of patchy stomatal
466 responses to humidity. Plant, Cell & Environment 20: 1087–1097.
467

Haworth M, Marino G, Materassi A, Raschi A, Scutt CP, Centritto M. 2023. The functional significance of the stomatal size to density relationship: interaction with atmospheric CO_2 and role in plant physiological behaviour. Science of the Total Environment 863: 160908.

Hetherington AM, Woodward FI. 2003. The role of stomata in sensing and driving environmental change. Nature 424: 901–908.

Hill KE, Guerin GR, Hill RS & Watling JR. 2015. Temperature influences stomatal density and maximum potential water loss through stomata of *Dodonaea viscosa subsp. angustissima* along a latitude gradient in southern Australia. Australian Journal of Botany 62: 657-665.

Hoffman R, Jain AK. 1983. A test of randomness based on the minimal spanning tree. Pattern Recognition Letters 1: 175–180.

Illian J, Penttinen A, Stoyan H, Stoyan D. 2008. Statistical analysis and modelling of spatial point patterns. West Sussex, UK: John Wiley & Sons.

Jaillet P. 1993. Rate of convergence for the Euclidean minimum spanning tree limit law. Operations Research Letters 14: 73–78.

Jones CL, Lonergan GT, Mainwaring DE. 1996. Minimal spanning tree analysis of fungal spore spatial patterns. Bioimages 4: 91–98.

Lawson T, McElwain JC. 2016. Evolutionary trade-offs in stomatal spacing. New Phytologist 210: 1149–1151.

Matkowski H, Daszkowska-Golec A. 2023. Update on stomata development and action under abiotic stress. Frontiers in Plant Science 14: 1270180.

Matos IS, Vu B, Mann J, Xie E, Madhavan S, Sharma S et al. 2025. Leaf venation network evolution across clades and scales. Nature Plants 11: 1–15.

McKown AD, Guy RD, Quamme L, Klápště J, La Mantia J, Constabel CP et al. 2014. Association genetics, geography and ecophysiology link stomatal patterning in *Populus trichocarpa* with carbon gain and disease resistance trade-offs. Molecular Ecology 23: 5771–5790.

Mott KA, Denne F, Powell J. 1997. Interactions among stomata in response to perturbations in humidity. Plant, Cell & Environment 20: 1098–1107.

Naulin PI, Valenzuela G, Estay SA. 2017. Size matters: point pattern analysis biases the estimation of spatial properties of stomata distribution. New Phytologist 213: 1956–1960.

Prim RC. 1957. Shortest connection network and some generalizations. Bell System Technical Journal 36: 1389–1401.

Quadros A. 2025. emstreeR: Tools for fast computing and plotting Euclidean minimum spanning trees. R package version 3.0.0.

R Core Team. 2025. R: A language and environment for statistical computing. Vienna, Austria: R Foundation for Statistical Computing. Available at: https://www.R-project.org/

Rasband WS. 1997. ImageJ software. Bethesda, MD, USA: National Institutes of Health.

Sachs T. 1991. Pattern formation in plant tissues. Cambridge, UK: Cambridge University Press.

Santibáñez F. 2017. Atlas agroclimático de Chile: Estado actual y tendencias del clima. Santiago, Chile: Universidad de Chile, Facultad de Ciencias Agronómicas, FIA.

Schneider CA, Rasband WS, Eliceiri KW. 2012. NIH Image to ImageJ: 25 years of image analysis. Nature Methods 9: 671–675.

Serna L, Fenoll C. 1997. Tracing the ontogeny of stomatal clusters in Arabidopsis with molecular markers. The Plant Journal 12: 747–755.

Simberloff D. 1979. Nearest neighbor assessments of spatial configurations of circles rather than points. Ecology 60: 679–685.

Uhl D, Kerp H. 2005. Variability of stomatal density and index in the Upper Permian conifer Quadrocladus Mädler—a taphonomical case study. Palaeogeography, Palaeoclimatology, Palaeoecology 218: 205–215.

Urban DL, Keitt TH. 2001. Landscape connectedness: a graph theoretic perspective. Ecology 82: 1205–1218.

Wallet F, Dussert C. 1997. Multifactorial comparative study of spatial point pattern analysis methods. Journal of Theoretical Biology 187: 437–447.

Wu HI, Rykiel EJ, Sharpe PJ, Zou G. 1987. A statistical physics approach to nearest neighbor distribution for individuals of finite size. Ecological Modelling 36: 73–87.

Xiong D, Flexas J. 2020. From one side to two sides: the effects of stomatal distribution on photosynthesis. New Phytologist 228: 1754–1766.

Yang KT, Chen GP, Xian JR. 2023. Stomatal distribution pattern for 90 species in Loess Plateau–based on replicated spatial analysis. Ecological Indicators 148: 110120.

Zhang L, Niu H, Wang S, Zhu X, Luo C, Li Y, Zhao X. 2012. Gene or environment? Species-specific control of stomatal density and length. Ecology and Evolution 2: 1065–1070.

Figure captions

Figure 1. Relationship between observed and predicted MST lengths across all samples. MST length was rescaled to millimeters. Each point represents a sample, with blue indicating Antumapu and red indicating Frutillar. The diagonal line denotes the 1:1 relationship, representing a perfect fit between observed and predicted values based on the theoretical model.

Figure 2. Comparison of observed MST length values (red points) with simulated distributions under clustered (blue), random (green), and over-dispersed (black) spatial scenarios for each sample from the Frutillar site. The x-axis shows sample identifiers, with the number of stomata in each sample indicated by small numbers above the axis. Bars represent the median and 95% confidence interval of the MST length from 1,000 simulations per spatial pattern scenario.

Figure 3. Comparison of observed MST length values (red points) with simulated distributions under clustered (blue), random (green), and over-dispersed (black) spatial scenarios for each sample from the Antumapu site. The x-axis shows sample identifiers, with the number of stomata in each sample indicated by small numbers above the axis. Bars represent the median and 95% confidence interval of the MST length from 1,000 simulations per spatial pattern scenario.

Figure 1.

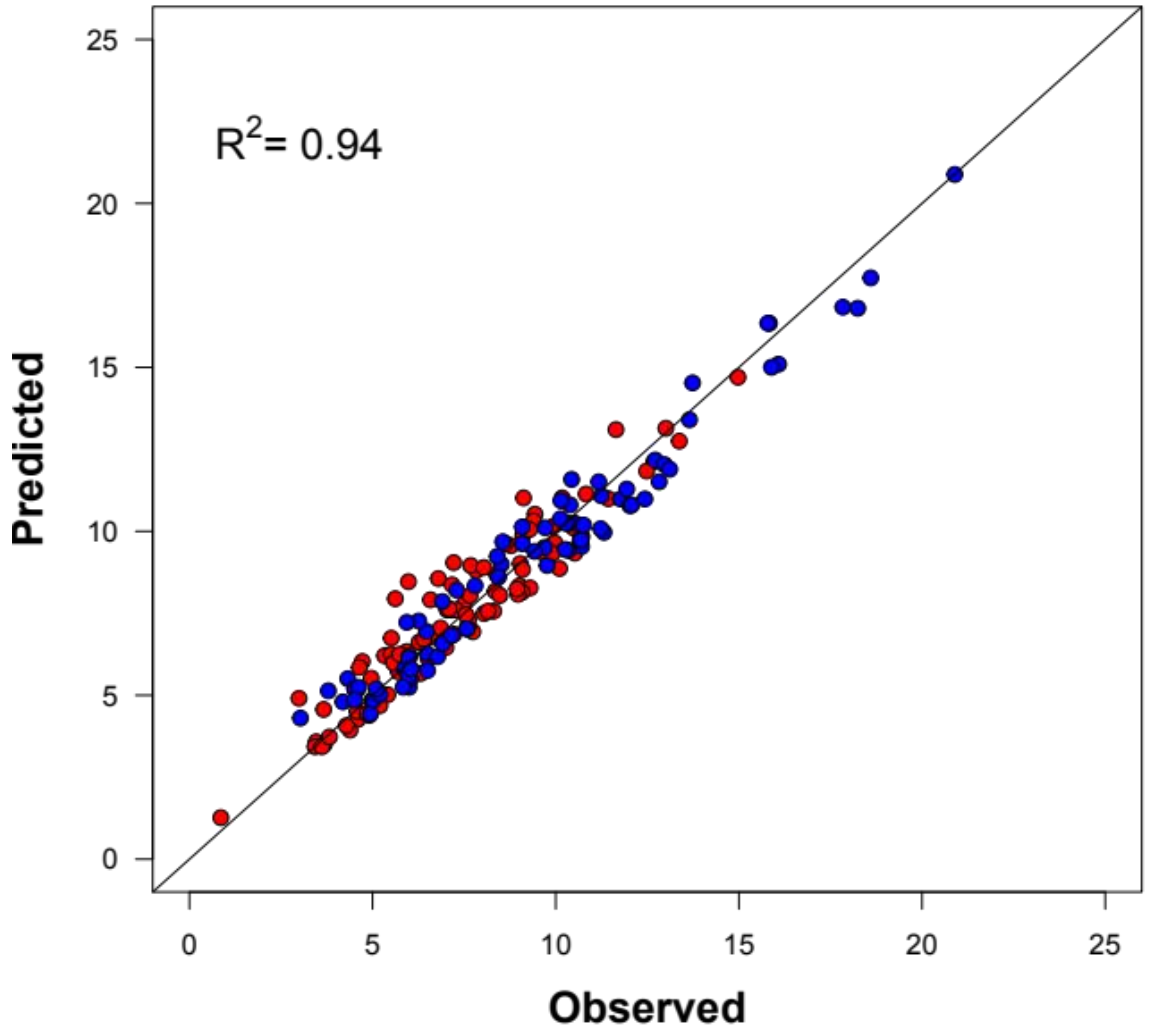

Figure 2.

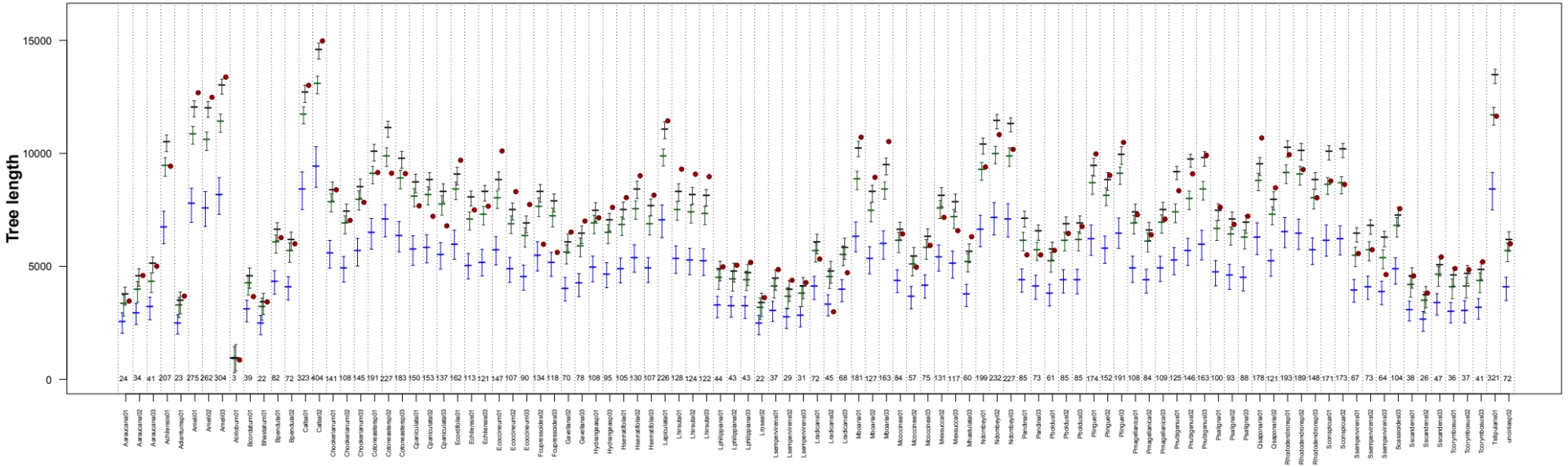

Figure 3.

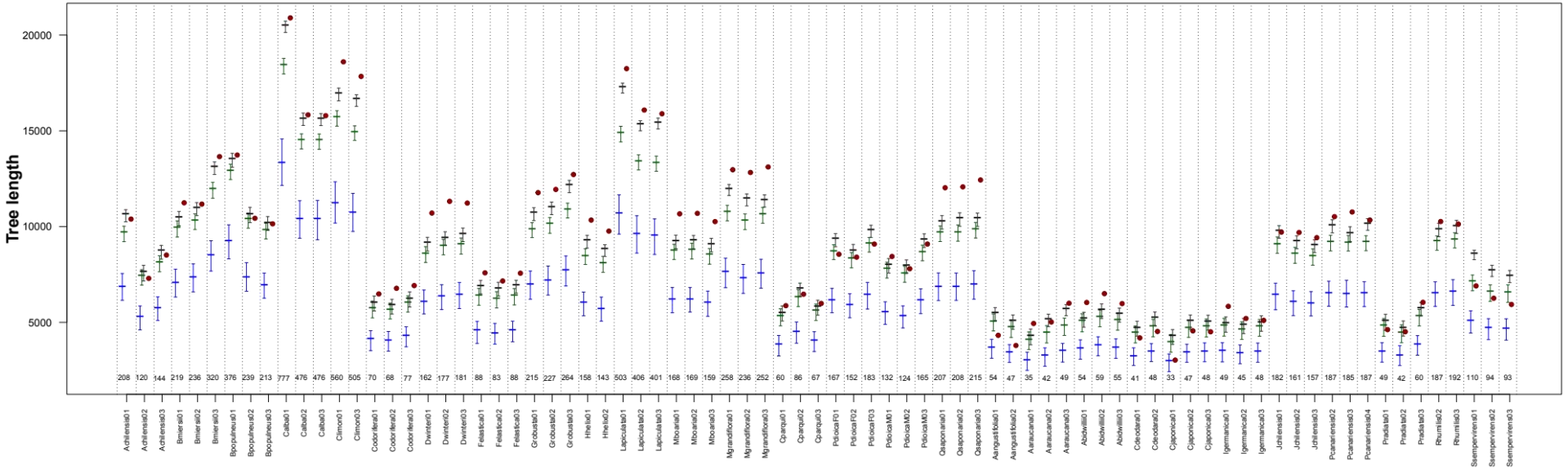
Tree length
20000
15000
10000
5000
208 120 144 219 236 320 376 239 213 777 476 476 560 505 70 68 77 162 177 181 88 83 88 215 227 264 158 143 503 406 401 168 169 159 258 236 252 60 86 67 167 152 183 132 124 165 207 208 215 54 47 35 42 49 54 59 55 41 48 33 47 48 49 45 48 182 161 157 187 185 187 49 42 60 187 192 110 94 93
Achilensis01
Achilensis02
Achilensis03
Bmiersii01
Bmiersii02
Bmiersii03
Bpopulifeus01
Bpopulifeus02
Bpopulifeus03
Calba01
Calba02
Calba03
Climon01
Climon03
Codorifera01
Codorifera02
Codorifera03
Dwinteri01
Dwinteri02
Dwinteri03
Felasticia01
Felasticia02
Felasticia03
Grobusta01
Grobusta02
Grobusta03
Hhelix01
Hhelix02
Lapiculata01
Lapiculata02
Lapiculata03
Mbovaria01
Mbovaria02
Mbovaria03
Mgrandiflora01
Mgrandiflora02
Mgrandiflora03
Cparqu01
Cparqu02
Cparqu03
PdoicicaF01
PdoicicaF02
PdoicicaF03
PdoicicaM01
PdoicicaM02
PdoicicaM03
Qlaponaria01
Qlaponaria02
Qlaponaria03
Aangustifolia01
Aangustifolia02
Aaraucana01
Aaraucana02
Aaraucana03
Abidwillii01
Abidwillii02
Abidwillii03
Cdeodara01
Cdeodara02
Cjaponica01
Cjaponica02
Cjaponica03
Igermanica01
Igermanica02
Igermanica03
Jchilensis01
Jchilensis02
Jchilensis03
Pcanariensis02
Pcanariensis03
Pcanariensis04
Pradiata01
Pradiata02
Pradiata03
Rhumilis02
Rhumilis03
Ssempervirens01
Ssempervirens02
Ssempervirens03